Dynamics of intracellular neonatal Fc receptor–ligand interactions in primary macrophages using biophysical fluorescence techniques

Andreas Pannek[a,b], Fiona J. Houghton[a], Anne M. Verhagen[c], Steven K. Dower[c], Elizabeth Hinde[d,e,*], and Paul A. Gleeson[a,*]

[a]Department of Biochemistry and Pharmacology and Bio21 Molecular Science and Biotechnology Institute, [d]School of Physics and Bio21 Molecular Science and Biotechnology Institute, and [e]Department of Biochemistry and Pharmacology, The University of Melbourne, Victoria 3010, Australia; [b]Institute of Experimental Immunology, University of Bonn, Venusberg Campus, D-53127, Germany; [c]CSL Limited, Research, Bio21 Molecular Science and Biotechnology Institute, Victoria 3010, Australia

ABSTRACT **The neonatal Fc receptor (FcRn) is responsible for the recycling of endocytosed albumin and IgG, and contributes to their long plasma half-life. We recently identified an FcRn-dependent recycling pathway from macropinosomes in macrophages; however, little is known about the dynamics of intracellular FcRn–ligand interactions to promote recycling. Here we demonstrate a multiplexed biophysical fluorescent microscopy approach to resolve the spatiotemporal dynamics of albumin–FcRn interactions in living bone marrow–derived macrophages (BMDMs). We used the phasor approach to fluorescence lifetime imaging microscopy (FLIM) of Förster resonance energy transfer (FRET) to detect the interaction of a FcRn–mCherry fusion protein with endocytosed Alexa Fluor 488–labeled human serum albumin (HSA–AF488) in BMDMs, and raster image correlation spectroscopy (RICS) analysis of single fluorescent-labeled albumin molecules to monitor the diffusion kinetics of internalized albumin. Our data identified a major fraction of immobile HSA–AF488 molecules in endosomal structures of human FcRn-positive mouse macrophages and an increase in FLIM-FRET following endocytosis, including detection of FRET in tubular-like structures. A nonbinding mutant of albumin showed minimum FLIM-FRET and high mobility. These data reveal the kinetics of FcRn–ligand binding within endosomal structures for recruitment into transport carriers for recycling. These approaches have wide applicability for analyses of intracellular ligand–receptor interactions.**

Monitoring Editor
Mary Munson
University of Massachusetts Medical School

Received: Feb 10, 2021
Revised: Oct 19, 2021
Accepted: Oct 25, 2021

INTRODUCTION

Many receptors recycle between the surfaces of cells and intracellular compartments (Cullen and Steinberg, 2018). The sites of interactions between receptors and ligands vary depending on the particular receptor. For some receptors, interactions with the ligand occur not only at the cell surface but also within endosomal compartments, and the interactions within endosomes play key roles in receptor function, for example, that of toll-like receptor 4 (TLR4; Racine and Bell, 2008; Gangloff, 2012) and G protein–coupled

This article was published online ahead of print in MBoC in Press (http://www.molbiolcell.org/cgi/doi/10.1091/mbc.E21-02-0061) on November 3, 2021.

Author contributions: A.P., A.M.V., S.K.D., E.H., and P.A.G. conceived the project, designed the experiments, and interpreted the data. A.P., F.J.H., and E.H. performed the majority of experiments and, with P.A.G., analyzed the data. A.M.V. and S.K.D. provided critical reagents. A.P., E.H., and P.A.G. wrote the original draft and A.M.V., S.K.D., and F.J.H. contributed to reviewing and editing.

Competing financial interest: S.K.D. and A.M.V. are employees of CSL Limited and are able to partake in employee share option schemes. Research funding from CSL Limited is provided through an Australian Research Council linkage grant collaboration.

*Address correspondence to: Elizabeth Hinde (elizabeth.hinde@unimelb.edu.au); Paul Gleeson (pgleeson@unimelb.edu.au).

Abbreviations used: BMDM, bone-marrow derived macrophages; CSF, colony stimulating factor; FcRn, neonatal Fc receptor; FFS, fluorescence fluctuation spectroscopy; FLIM, fluorescence lifetime imaging microscopy; FRET, Förster resonance energy transfer; hFcRn$^{Tg/Tg}$, mFcRn$^{-/-}$ hFcRn$^{Tg/Tg}$; HSA, human serum albumin; HSA-AF488, Alexa Fluor 488-HSA; B2M, β2 microglobulin; PFA, paraformaldehyde; RICS, raster image correlation spectroscopy; SFM, serum-free medium.

receptors (Hanyaloglu, 2018; Retamal *et al.*, 2019). In some instances, interactions between recycling receptors and ligands occurs selectively within intracellular compartments following endocytic uptake of the ligand. One example of a recycling receptor where the ligand interaction occurs exclusively within intracellular compartments is the neonatal Fc receptor (FcRn), a major histocompatibility complex (MHC) class-I like molecule (Tesar and Bjorkman, 2010). FcRn plays an important role in both neonatal and adult life; in the adult, FcRn rescues endocytosed IgG and albumin from lysosomal degradation by capturing these ligands in acidic endosomes, before their delivery to lysosomes, and recycling them back to the cell surface, where they dissociate at neutral pH and are released, thereby extending their lifetime within the circulation (Roopenian and Akilesh, 2007; Ward and Ober, 2009). Identifying the interactions between FcRn and ligands in space and time within these intracellular compartments is important in defining the cell biology and molecular dynamics of the FcRn recycling system.

FcRn is a membrane-bound heterodimer consisting of an MHC class I–like heavy chain (~40 kDa) and a noncovalent light chain, β2 microglobulin (β2m), which is common to all MHC class I molecules. The FcRn-binding sites for albumin and IgG differ, but both involve pH-dependent salt bridges mediated by histidine residues (Andersen *et al.*, 2012; Ward and Ober, 2009). At physiological pH, histidine is not ionized and FcRn does not interact with ligands (Martin *et al.*, 2001). The pH dependence of FcRn binding to ligands is one factor that defines the intracellular locations where the interaction takes place. FcRn ligands are internalized into cells predominantly by fluid phase endocytosis (Lim and Gleeson, 2011; Lim *et al.*, 2015). Previously we have shown that human albumin (HSA) is internalized by macropinocytosis by primary macrophages, a very efficient, nonselective pathway for uptake of soluble molecules (Toh *et al.*, 2019). In addition, we demonstrated that albumin was recycled, in an FcRn-dependent manner, by a fast and efficient recycling pathway from newly formed macropinosomes. Tubules that emerged from early macropinosomes contained HSA ligand, and these tubules then formed transport carriers projecting to the plasma membrane for recycling HSA (Toh *et al.*, 2019). An FcRn-nonbinding mutant of HSA was internalized efficiently by primary macrophages but was absent from the emerging transport carriers from these early macropinosomes and was transported to the lysosomes for rapid degradation (Toh *et al.*, 2019).

A key unanswered question is the relationship between the albumin recycling pathway and the temporal and spatial events associated with its interaction with FcRn. A major challenge in identifying interactions between ligands and membrane receptors within intracellular compartments, compared with the cell surface, is that such interactions need to be detected and quantified in the presence of an unbound pool of ligand. To this end, here we used two independent biophysical approaches to monitor the intracellular interaction of HSA with the membrane-bound FcRn following endocytosis of ligand. First, the phasor approach to fluorescence lifetime imaging microscopy (FLIM) of Förster resonance energy transfer (FRET) (Digman *et al.*, 2008; Hinde *et al.*, 2012). FLIM detects the fluorescence lifetime of the donor fluorophore, which upon close proximity to an acceptor fluorophore will decrease due to FRET, and the phasor approach to FLIM analysis is a quantitative method for detection of FRET in the presence of fluorescence artifacts inherent in the cellular environment (Hinde *et al.*, 2012). Second, we used a novel approach to fluorescence fluctuation spectroscopy (FFS) called raster image correlation spectroscopy (RICS; Digman *et al.*, 2005; Digman and Gratton, 2011; Priest *et al.*, 2019), which together with FLIM-FRET enables assessment of the direct interaction of albumin with FcRn, as well as of the mobility of the bound versus unbound ligand. Findings from these studies reveal rapid binding of HSA to FcRn following internalization and the presence of the bound ligand–FcRn complex in endosomal structures and tubules emerging from endosome bodies.

RESULTS

Generation of functional fluorescent-tagged albumin and FcRn constructs

To quantify the interaction of intracellular FcRn with the endocytosed ligand, albumin, and the impact endogenous FcRn binding has on albumin mobility, we used FLIM-FRET and RICS, respectively. Both techniques rely on fluorescently tagged human albumin (either HSA–AF488 or HSA–AF568). FLIM-FRET also required a fluorescently tagged FcRn that, based on the spectrum, would undergo FRET with HSA, while RICS required a fluorescently tagged FcRn nonbinding mutant of HSA, spectrally distinct from wild-type (wt) HSA. For the FLIM-FRET experiment we employed HSA–AF488 (green) and generated mCherry (red) fused to either the N-terminus or C-terminal cytoplasmic tail of the heavy chain of human FcRn. The human FcRn constructs included the β2m light chain in a polycistronic plasmid, with the FcRn alpha chain following β2m to optimize the assembly of transport-competent mCherry fusions in the ER, as described in *Materials and Methods*. Because both N-terminal and C-terminal mCherry constructs placed the donor–acceptor fluorophores within the Förster distance of <10 nm and as the C-terminal tagged construct (FcRn–mCherry) (Figure 1A) exhibited stable expression, this construct was used throughout the studies described, except where stated otherwise. We initially demonstrated that the FcRn–mCherry fusion protein was the correct size and localized to endosome-like structures in transfected HeLa cells (Figure 1, B and C). The localization of FcRn–mCherry was further analyzed by staining FcRn–mCherry transfected cells with markers of the early (EEA1) and recycling (Rab11) endosomes, ER/intermediate compartment (KDEL–receptor), late endosomes (CD63), and Golgi (GM130; Figure 2). FcRn–mCherry showed partial colocalization with both the early endosome marker (EEA1) and the recycling endosome marker (Rab11) and little overlap with ER, Golgi, and late endosome markers. Hence, the distribution of human FcRn tagged with mCherry in HeLa cells demonstrates efficient transport from the ER and Golgi to endosomal compartments and is consistent with intracellular distribution of the untagged human FcRn, which is located predominantly at early and recycling endosomes (Toh *et al.*, 2019).

To analyze whether the FcRn–mCherry fusion protein was functional, and as fluid phase endocytosis is inefficient in cultured HeLa cells, we used a strategy previously adopted by our laboratories for cultured HEK cells (Chia *et al.*, 2018), namely, incubation of transfected cells with human albumin (HSA) under acidic conditions to allow ligand binding to cell surface FcRn–mCherry receptors followed by internalization by receptor-mediated endocytosis. HSA–AF488 was efficiently bound at 4°C under acidic conditions and endocytosed at 37°C (Figure 1D). In addition, surface-bound HSA–AF488 and internalized HSA–AF488 showed a strong FLIM-FRET signal in FcRn–mCherry expressing cells, demonstrating that the receptor–ligand fluorescent probes mediate a FLIM-FRET signal following interaction (Figure 1D). Using this assay, next we compared the binding and uptake of wt HSA–AF488 with an FcRn nonbinding mutant of HSA, rHSA^{H464Q}–AF488, over a pH range of 5.0–7.0. HSA–AF488 was efficiently endocytosed under acidic conditions, that is, at pH 6.0 and lower (Figure 3), whereas the nonbinding mutant, rHSA^{H464Q}– AF488, was very poorly taken up by FcRn–mCherry

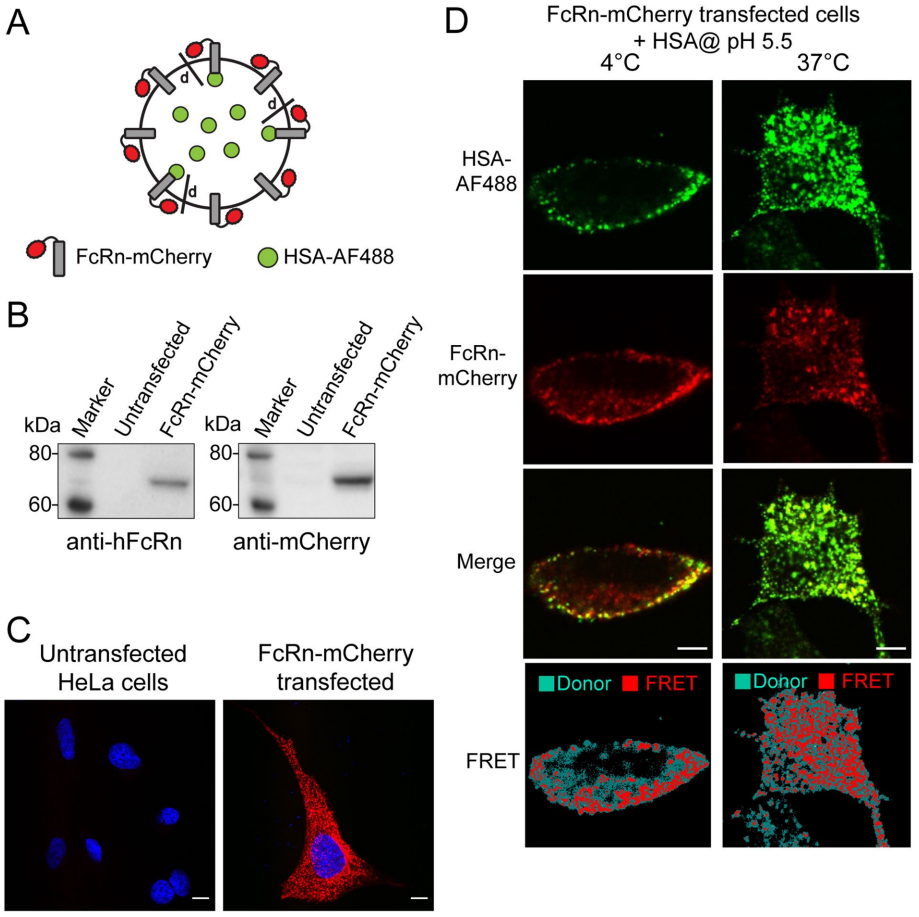

FIGURE 1: FLIM-FRET analysis of AF488-labeled HSA in transfected HeLa cells expressing C-terminal labeled FcRn–mCherry fusion protein. (A) Cartoon showing the membrane FcRn (gray) and mCherry (red) and the ligand HSA–AF488 ligand (green). FRET efficiency is dependent on the distance (*d*, nm) between the two fluorophores. (B, C) HeLa cells were transfected with the polycistronic pIRES construct expressing β2M and FcRn–mCherry fusion protein. Immunoblotting with anti-FcRn and mCherry antibodies detected a band of the expected 70-kDa size, B, and confocal image of mCherry fluorescence, C. (D) FcRn–mCherry transfected HeLa cells were pulsed with HSA–AF488 for 1 h on ice, or for 15 min at 37°C, in pH 5.5 buffer. Monolayers were washed and fixed in 4% PFA. Confocal images (top three rows), as indicated, were acquired with an Olympus FV3000 confocal microscope. Data for calculation of FRET-transfer efficiency (bottom panels) were acquired with an Olympus FV3000 confocal microscope using a FLIM-FRET detector. Scale bar, 10 μm.

transfected cells over the pH range 5.0–7.0, indicating pH-dependent binding of HSA–AF488 to FcRn–mCherry (Figure 3). As the intracellular interaction of FcRn–mCherry and HSA–AF488 occurs in acidic compartments, we analyzed the FRET donor probe, HSA–AF488, independently under acidic conditions in solution. No change in the lifetime of the donor probe was observed over the pH range 5.0–7.0 (unpublished data), demonstrating that the system was viable for the intracellular conditions required for receptor–ligand interactions.

Next, we evaluated the capacity of FLIM analysis to detect FRET upon HSA–AF488 interaction with FcRn labeled with mCherry on the N-terminus versus the C-terminus (Figure 4A). Here we quantified the FLIM data using the phasor approach, which transforms the fluorescence lifetime recorded in each pixel into a two-dimensional plot known as the phasor plot. To perform this experiment, HSA–AF488 (donor molecule) was bound at 4°C to the cell surfaces of HeLa cells transfected with one of the FcRn fusions with mCherry (acceptor molecule) under acidic conditions and then internalized by receptor-mediated endocytosis at 37°C for 15 min (Figure 4, B and C). This protocol led to high levels of HSA–AF488 being endocytosed, which showed a punctate endosomal staining similar to the expressed FcRn-mCherry constructs. The unquenched fluorescence lifetime of the donor molecule was then analyzed in untransfected HeLa cells incubated with HSA–AF488 for 4 h where the ligand was slowly taken up by fluid-phase endocytosis into large endocytic structures, to establish the baseline from which FRET interaction with mCherry–FcRn or FcRn–mCherry could be detected in the transfected HeLa cells (Figure 4D). The phasor distribution of this donor control (centered within the teal cursor, Figure 4D) revealed the unquenched fluorescence lifetime of HSA–AF488 to be ~3.2 ns and enabled extrapolation of a FRET trajectory (curved black line, Figure 4D) to characterize the FRET efficiency of interaction with the FcRn mCherry constructs in the presence of background signal (contained within black cursor, Figure 4D). Specifically, from superimposition of the phasor distribution of HSA–AF488 in the presence of mCherry–FcRn (centered within yellow cursor, Figure 4D) versus FcRn–mCherry (centered within red cursor, Figure 4D) over the donor control–generated FRET trajectory, we find that HSA–AF488 interaction with mCherry–FcRn results in a high FRET efficiency (20–30%) that significantly quenches the donor lifetime to ~2.2 ns and that HSA–AF488 interaction with FcRn-mCherry results in a moderate FRET efficiency (10–20%) that quenches the donor lifetime to ~2.5 ns. The phasor plot and fluorescent image are linked; therefore, the donor pixel lifetimes from the phasor plot can be spatially mapped on the cell image (Figure 4E). The result from these experiments, which is clearly observed upon pseudocoloring the FLIM acquisitions of these different donor–acceptor experiments (Figure 4E) on the image, according to the FRET states identified along the FRET trajectory (Figure 4D), is consistent with the difference in Förster distance between the different donor–acceptor locations with respect to the endosomal membrane (schematic shown in Figure 4A). Thus, both the N-terminal mCherry–FcRn construct and the C-terminal FcRn–mCherry construct have the potential to quantitatively assess FcRn–HSA interactions. We used the C-terminal FcRn–mCherry construct for subsequent analysis of primary macrophages, as the levels of expression were adequate compared with only very low levels of expression of the N-terminal mCherry–FcRn construct in macrophages.

FLIM-FRET analysis of FcRn–ligand interaction in endosomes of primary macrophages

Having established that the FLIM-FRET system was viable, we then transduced mouse FcRn-knockout (FcRn-KO) bone marrow–derived

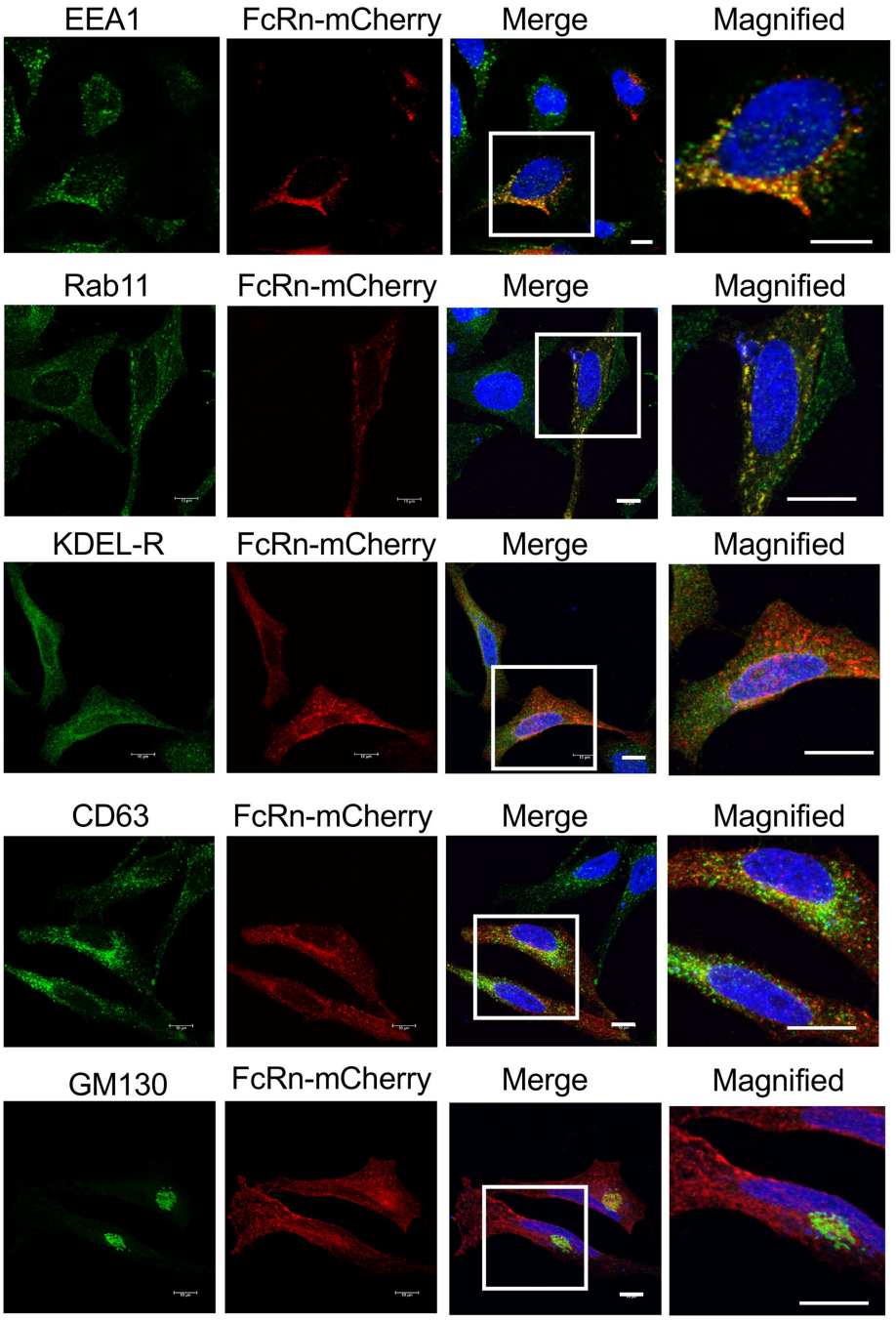

FIGURE 2: Intracellular distribution of FcRn-mCherry in transfected HeLa cells. HeLa cells were transfected with the polycistronic pIRES construct expressing β2M and FcRn–mCherry fusion protein for 48 h. Cells were fixed, permeabilized, and stained with the organelle markers (green) EEA1 (early endosomes), Rab11 (recycling endosomes), KDEL receptor (KDEL-R; ER/intermediate compartment), CD63 (late endosomes), and GM130 (Golgi), as indicated. Boxed regions in merged images are shown magnified. Bars represent 10 μm.

macrophages (BMDMs) with recombinant FcRn–mCherry lentivirus. Transduced macrophages with modest levels of FcRn–mCherry expression were selected for the subsequent studies. The distribution of human FcRn–mCherry in transduced BMDMs showed a punctate staining pattern and overlap with the early endosome marker SNX5. There was very little mCherry fluorescence that overlapped with the ER marker KDEL (Figure 5A), indicating that the fluorescently tagged FcRn protein was transported efficiently from the ER after synthesis. To confirm that endocytosed HSA is delivered to an endosomal compartment positive for FcRn–mCherry, transduced BMDM were pulsed with HSA–AF488 for 15 min and the cells fixed with PFA. Endocytosed HSA–AF488 was detected in endosomal puncta scattered throughout the cytoplasm, and many of the puncta showed overlap with FcRn–mCherry (Figure 5B), demonstrating that the FcRn fusion protein was located in the same compartment(s) as the endocytosed HSA in BMDM, and providing a system to examine the intracellular interactions of this ligand–receptor complex in primary cells.

We then performed a series of FLIM-FRET experiments recording the FcRn–ligand interaction in endosomes of the BMDMs (Figure 6A). Transduced and non-transduced FcRn-KO BMDMs were activated with CSF-1 to induce macropinocytosis (Lim *et al.*, 2015) and pulsed with either HSA–AF488 or the FcRn nonbinding HSA mutant rHSA^{H464Q}–AF488 (donor molecules), in the absence versus presence of FcRn–mCherry (Figure 6, B and C) for 5 min, and a FLIM-FRET experiment was performed after a 20-min incubation period (Figure 6, D amd F), since at this time point, the donor fluorescence lifetime was found to stabilize (Figure 7). In particular, from phasor analysis of FLIM-FRET experiments performed over a time course, based on our previous studies, which tracked the location and recycling of endocytosed albumin in the presence and absence of FcRn (Toh *et al.*, 2019; Supplemental Figure S1), we found that 1) HSA-AF488 alone (donor only) underwent an initial change in fluorescence lifetime to 3.2 ns (likely due to changes in intracellular environment) that was maintained from 20 min onward (i.e., ~0% FRET pixels; Figure 7A), and 2) HSA–AF488 in the presence of FcRn–mCherry (FRET experiment) maintained a quenched lifetime of 2.5 ns (moderate FRET as defined in Figure 4) beyond 20 min that is highly likely to be the result of a ligand–receptor interaction (i.e., ~20% FRET pixels; Figure 7B). As individual donor molecules are either undergoing FRET or not, the phasor plot trajectory shows the proportion of the donor population that is actively undergoing FRET—for example, has a quenched lifetime of 2.5 ns—and in Figure 7B shows that ~20% of the donor pixels are undergoing FRET. This conclusion is supported by the finding that the nonbinding mutant rHSA^{H464Q}–AF488, in the presence of FcRn–mCherry, underwent the same change in fluorescence lifetime as the donor control (Figure 7C) and did not exhibit a detectable ligand–receptor interaction (i.e., ~0% FRET).

From quantitation of multiple FLIM-FRET experiments after 20 min incubation, where both HSA–AF488 and rHSA^{H464Q}–AF488

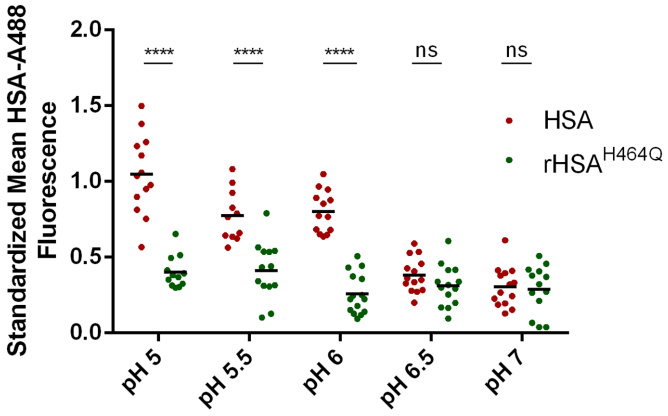

FIGURE 3: pH-dependent binding of HSA–AF488 to FcRn–mCherry. HeLa cells were transfected with the polycistronic pIRES construct expressing FcRn–mCherry fusion protein and β2M. FcRn–mCherry expressing HeLa cells were incubated with 100 μg/ml HSA–AF488 in buffer with a pH from 5.0 to 7.0, as indicated, for 15 min. Cells were then washed, fixed, and analyzed by confocal microscopy. Fluorescence is expressed as a ratio of the mean fluorescence within cells in the green and red channels. Each symbol represents an individual sample. Filled red symbols, HSA–AF488; green symbols, nonbinding mutant rHSA^{H464Q}–AF488. Means are shown. $n \geq 11$. Data analyzed by unpaired two-tailed Student *t* test. **** $p < 0.0001$.

were efficiently internalized into large globular structures, typical of macropinosomes, in FcRn–mCherry positive BMDM (Figure 6, B and C), and which showed considerable overlap with the FcRn–mCherry fusion protein (Supplemental Figure S2), we found the efficiency of FRET interaction between HSA and FcRn to be 21% (Figure 6D). This was also the FRET level initially observed in Figure 4 for this biosensor in HeLa cells. Pseudo-coloring the FLIM acquisitions on the image, according to either the unquenched donor (within the teal circle) or the quenched donor (within the red circle) along the FRET trajectory (Figure 6D), shows the FRET map for HSA and FcRn interactions within intracellular structures (Figure 6F). Quantitative analysis of the fraction of pixels undergoing FRET revealed a significantly higher fraction for HSA–AF488 and FcRn–mCherry than for the nonbinding mutant rHSA^{H464Q}–AF488 (Figure 6E). Thus, these data demonstrate a specific ligand interaction between HSA and FcRn after internalization into large endosomal structures. We have previously shown that internalized HSA–AF488 was detected in tubules emerging from early macropinosomes, which were then directed toward the plasma membrane, whereas in the absence of FcRn, HSA was neither partitioned into tubules nor recycled, but remained within the body of the macropinosome (Toh *et al.*, 2019). Notably, in FcRn–mCherry transduced BMDMs, HSA–AF488 was prominent not only in endosomal structures but also in thin tubular structures emanating from large endosomes (Figure 8), consistent with our previous findings (Toh *et al.*, 2019). At the 20-min and 25-min time points after endocytosis with stable fluorescent lifetime, FRET was detected in HSA–AF488 and FcRn–mCherry positive tubular-like structures (Figure 8, B and C). Based on the geometry and mobility, these tubular structures are reminiscent of emerging tubular carriers and the FRET detected indicates a FcRn–albumin interaction within these tubules. In contrast, FcRn–mCherry positive tubular structures were devoid of the nonbinding mutant rHSA^{H464Q}–AF488 (Supplemental Figure S3), consistent with our previous findings.

Raster image correlation spectroscopy of single albumin molecules

To further investigate the dynamics of the HSA–FcRn interaction, we next used an FFS-based method of analysis called RICS that can extract single-molecule information on HSA mobility and infer the fraction of HSA molecules bound to FcRn in a living cell. A major advantage of RICS is that it enables detection of the interaction of the HSA ligand with endogenous, nontagged FcRn. RICS extracts this information on HSA by spatially correlating the intensity signal that originates from a population of fluorescently labeled HSA molecules diffusing throughout a time series acquisition of intensity frames and fitting the resulting three-dimensional correlation profile to a diffusion model. We reasoned that unbound fluorescent HSA–AF488 molecules would be highly mobile in the lumen of endosomes and essentially undergo free diffusion, while fluorescent HSA molecules engaged with FcRn, its membrane receptor, would be transiently immobilized and exhibit a significantly lower apparent diffusion coefficient. Thus, by monitoring the fraction of HSA molecules exhibiting a low apparent diffusion coefficient, we could quantify the fraction of endocytosed ligand engaged with FcRn. To validate this assumption, we employed the FcRn nonbinding mutant rHSA^{H464Q}, which shows minimum interaction with intracellular FcRn, as demonstrated by FLIM-FRET (Figure 6), and performed a two-channel RICS analysis on BMDM from a FcRn-KO mouse transgenically expressing untagged human FcRn (hFcRn$^{Tg/Tg}$; Roopenian *et al.*, 2010); the BMDMs from hFcRn$^{Tg/Tg}$ mice were CSF-1 activated and incubated with 10 μg/ml both wt HSA–AF568 (red) and the FcRn nonbinding mutant rHSA^{H464Q}–AF488 (green; Figure 9A). Thus, binding of the ligand is monitored to an untagged receptor expressed endogenously rather than under transfection conditions.

Following uptake of the two fluorescent HSA conjugates, our RICS analysis workflow involved scanning a small region of interest (ROI) within a selected cell, rapidly as a function of time, in both the HSA–AF568 (red) and rHSA^{H464Q}–AF488 (green) channels, and then applying a moving average to the recorded fluctuations in fluorescence intensity to remove slow macromolecular movements of the endosomes internalizing the HSA conjugates (*Materials and Methods*) and calculating the RICS spatiotemporal correlation function (Figure 9, B and C). This resulted in two three-dimensional RICS profiles describing HSA–AF568 versus rHSA^{H464Q}–AF488 mobility that could each be fitted to a two-component diffusion model (Figure 9, D and E). The fits in each channel return an apparent diffusion coefficient (*D*) and amplitude (*G*) for a fast versus slow component that we interpret to describe the mobility and fraction of the free (G_{FREE}) versus FcRn bound (G_{BOUND}) HSA molecules, respectively. From performing this two-channel RICS analysis on multiple BMDM cells ($N = 5$), we find that while the mobility coefficients of the free (Figure 9F) and FcRn bound (Figure 9G) components of HSA–568 (red) versus rHSA^{H464Q}–AF488 (green) molecules are not significantly different, the fraction of HSA–568 molecules FcRn-bound (slow component) is significantly higher than that of rHSA^{H464Q}–AF488 (Figure 9H). This result confirms our interpretation of the two-component fit and reveals that while 45% of the HSA molecules are freely diffusing within the lumen of an endosome at a rate of 51 ± 7 μm^{2}s^{-1}, 55% of the HSA molecules are FcRn-bound, with an apparent mobility of 0.07 ± 0.02 μm^{2}s^{-1}, a significant difference from the freely diffusing population.

DISCUSSION

The ability to identify interactions between membrane receptors and ligands in space and time within intracellular compartments is important in defining cell-biological events associated with

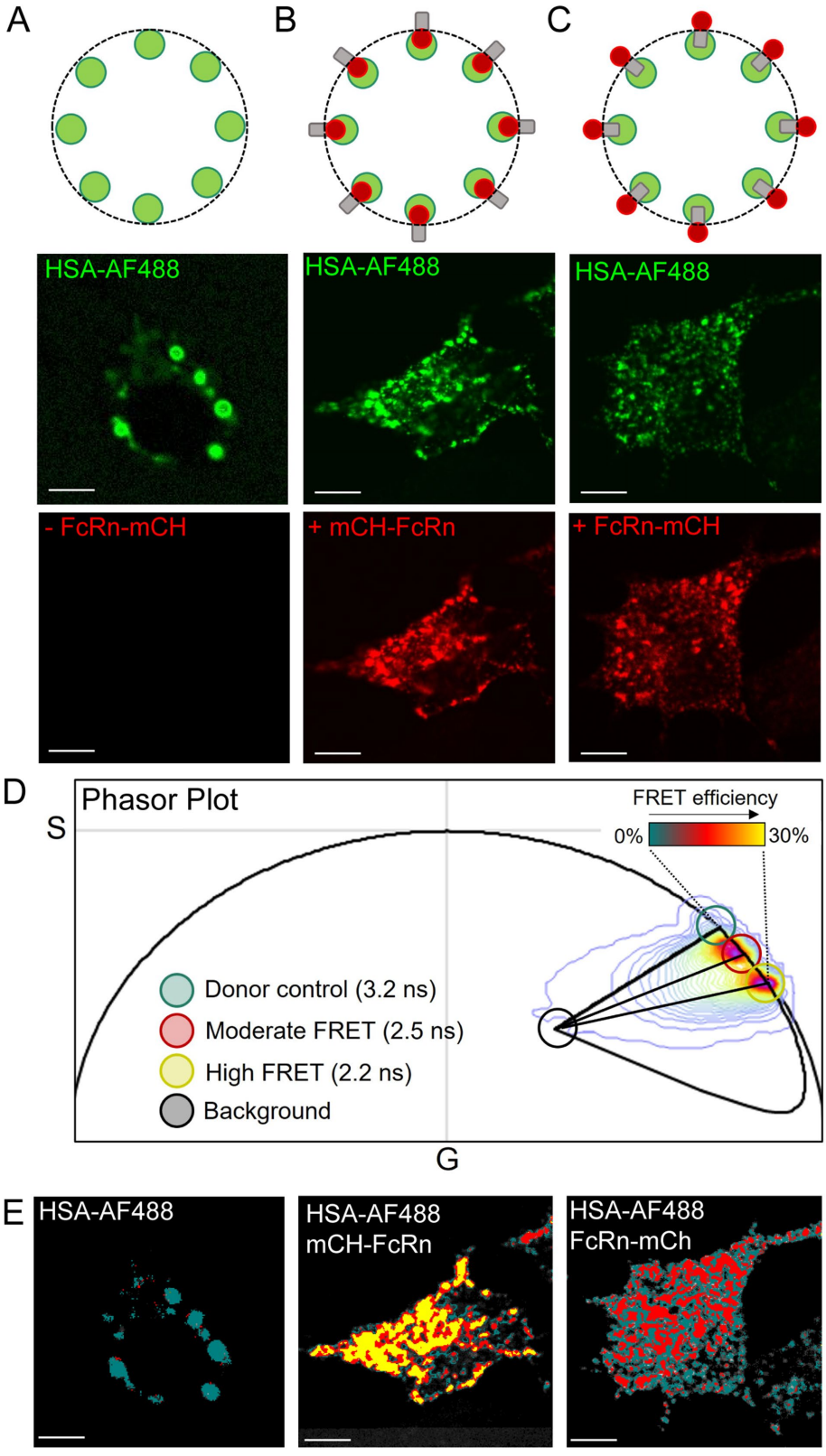

FIGURE 4: Comparison of FLIM of HSA–AF488 interaction with N-terminal and C-terminal FcRn fusions with mCherry by FRET detection. (A–C) Schematic of the donor control (HSA–AF488 labeled endosome) in the absence, A, versus presence of either N-terminal mCherry–FcRn (mCH–FcRn), B, or C-terminal FcRn–mCherry (FcRn–mCH), C. Untransfected HeLa cells were incubated with HSA–AF488 for 4 h at 37°C and HeLa cells transfected with mCherry–FcRn or FcRn–mCherry, as indicated, incubated with HSA–AF488 for 15 min at 37°C, in pH 5.5 buffer. Images are shown in the donor and acceptor channels. (D) Combined phasor distribution of HSA–AF488 (donor) lifetimes in the absence and presence of the FcRn–mCherry fusions (acceptor) with a theoretical FRET trajectory for the donor control superimposed. The distribution of pixel lifetimes is shown as a heat map. (E) FLIM images matched to A–C and pseudo-colored according to FRET (palette defined in D) reveal HSA to undergo significant interaction with both N-terminal and C-terminal FcRn fusions with mCherry. Scale bar, 5 μm.

intracellular membrane receptor interactions. A major challenge in identifying ligand–membrane receptor interactions within intracellular compartments, as distinct from the cell surface, has been that these interactions need to be detected and quantified in the presence of an unbound pool of ligand. Here we applied two independent biophysical techniques to detect the interaction of the soluble ligand albumin with its membrane receptor, FcRn, an interaction that requires an acidic endosomal environment, within primary mouse macrophages. The use of biophysical techniques to probe interactions in primary cells has broad application to a variety of physiological systems and is particularly relevant to our studies on albumin uptake and interaction with FcRn. Macropinocytosis is the major pathway for endocytic uptake of FcRn soluble ligands, a pathway particularly active in primary cells, especially immune cells (Lim and Gleeson, 2011). Previously, we demonstrated that albumin is rapidly internalized by fluid-phase macropinocytosis in primary macrophages and recycled in an FcRn-dependent manner (Toh *et al.*, 2019). By multiplexed biophysical fluorescent microscopy here, we have shown a direct interaction of albumin with FcRn following uptake of albumin within endosomal structures. A strength of the approach used in our study was the inclusion of primary macrophages deficient in FcRn and the use of a nonbinding mutant of albumin (Andersen *et al.*, 2012) to demonstrate that the observed FRET and changes in ligand mobility was directly related to a ligand–receptor interaction.

The use of both FLIM-FRET and RICS provided complementary approaches that not only confirmed the detection of an interaction between ligand and receptor within endosomes but also provided additional information on the spatial dynamics of the interaction. Expression of FcRn–mCherry was modest and showed a distribution similar to that of endogenous FcRn in macrophages. FLIM-FRET detected ~27% of HSA to be bound to FcRn-mCherry (Figure 6E) with an

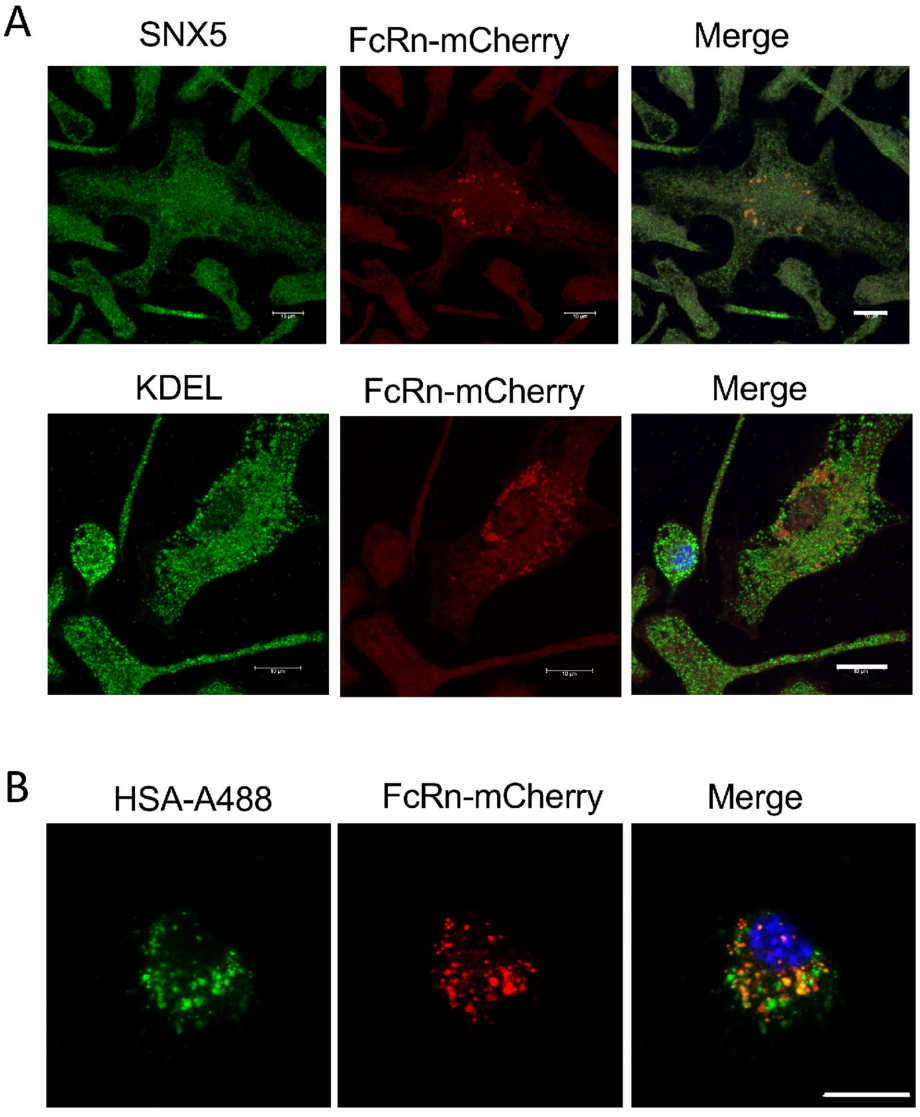

FIGURE 5: Intracellular distribution of FcRn–mCherry in transduced BMDMs. (A) FcRn-KO BMDM were transduced with recombinant FcRn–mCherry lentivirus as described in *Materials and Methods*, fixed, permeabilized, and stained with antibodies to SNX5 (early endosomes) or KDEL (ER marker) as indicated. (B) Transduced BMDM were incubated with HSA–AF488 at 37°C for 15 min to allow fluid phase endocytosis of HSA–AF488, and cells were fixed and stained with DAPI. The merged image shows the considerable overlap of internalized HSA with intracellular FcRn. Bars represent 10 µm.

efficiency of 21% ~20 min after uptake of HSA–AF488. We were unable to quantify the ligand binding at earlier time points due to a transient nonspecific change in the fluorescent lifetime of the donor fluorophore following endocytosis. This is likely due to the transition of the fluorophore between two different environments (extracellular versus acidic endosomal); a time course of the donor showed that the fluorescent lifetime stabilized after approximately 20 min. Therefore, the use of FLIM was particularly informative on the conditions within the endosomal system that were compatible with a specific FRET signal between HSA and FcRn. The detection of FRET within FcRn-positive tubular structures, albeit qualitative, is consistent with the recruitment of albumin in transport carriers for recycling to the cell surface and, together with our previous finding that HSA but not rHSA^{H464Q} was detected in tubules in live BMDM (Toh *et al.*, 2019), indicates that an interaction with FcRn is required for entry into these putative transport carriers. Confirmation of these findings with quantitative analysis on the FRET signals of HSA and FcRn within the tubular transport carriers would be instructive, although a technical challenge may be the gradual loss of acidity and the disruption of the ligand–receptor complex within the lumen of the tubules before arrival at the cell surface.

The expression of the fluorescently tagged FcRn–mCherry for FLIM-FRET experiments has the disadvantage of cells expressing the receptor at nonphysiological levels. Transduced BMDMs were selected that express only a modest level of FcRn–mCherry to minimize the impact of overexpression. In addition, the heterologously tagged FcRn showed an intracellular distribution compatible with the endogenous receptor (Toh *et al.*, 2019); therefore the interaction of FcRn–mCherry with albumin was in the appropriate location. The inclusion of a nonbinding HSA mutant as a control and the use of FLIM to resolve FRET from autofluorescence also minimizes artifacts from elevated levels of FcRn expression.

The application of RICS for detection of ligand-receptor engagement in endosomes is powerful, as we avoid the need for a tagged FcRn and enable detection of FcRn–HSA engagement at an endogenous level, in contrast to FLIM-FRET, which requires the fluorescently tagged FcRn. FLIM-FRET and RICS are independent techniques that are complementary, as they analyzed heterologous and endogenous FcRn interactions, respectively, with the HSA–AF488 ligand. Our findings from RICS analysis of fluorescently labeled wt HSA versus a HSA nonbinding mutant showed that the wt ligand's mobility can be described by a two-component diffusion model where the fast component reports on the fraction of ligand molecules freely diffusing within the lumen of the endosome, and the slow component reports the fraction of ligand receptor bound. The RICS data indicate that approximately 55% of HSA–AF488 molecules were bound to endogenous FcRn, and in agreement with FLIM-FRET, the rHSA^{H464Q} mutation reduces this fraction twofold. The observation that ~55% of HSA–AF488 molecules were bound to endogenous FcRn by this biophysical technique is consistent with our previous finding that 50% of the total internalized HSA–AF488 was recycled, in an FcRn-dependent manner, by hFcRn$^{Tg/Tg}$ BMDM (Toh *et al.*, 2019). A challenge in the application of RICS is the analysis of ligand–receptor interactions within endosomes, as the mobility of the ligand needs to be determined within the context of the relatively slowly mobile endosome structures. Future work will therefore be dedicated to coupling RICS analysis of ligand–receptor interaction with orbital tracking of endosomal movement (Begarani *et al.*, 2019).

In conclusion, the ability to detect interactions in intracellular compartments provides a biological assay to quantify and compare

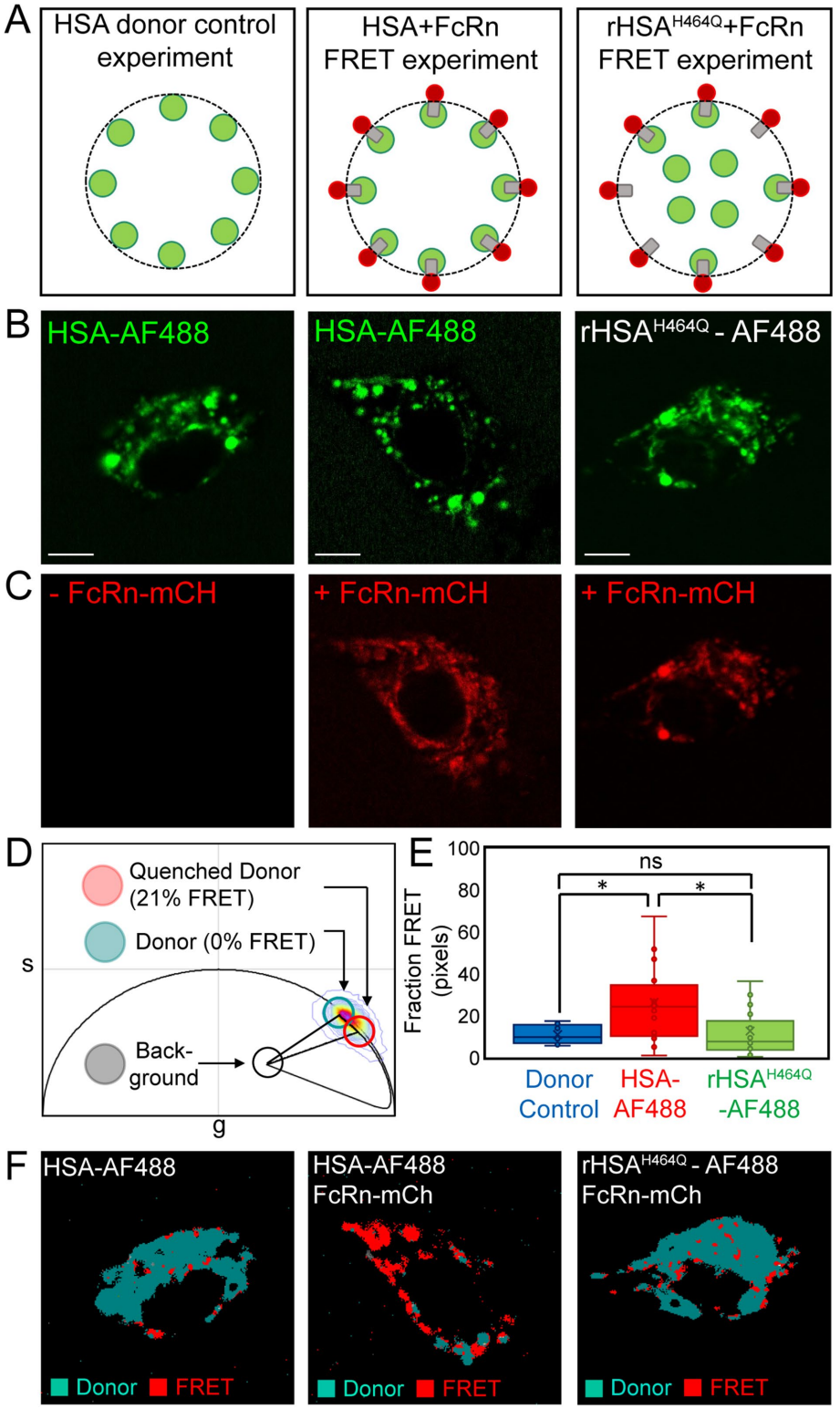

FIGURE 6: Fluorescence lifetime imaging microscopy (FLIM) of HSA–AF488 interaction with FcRn–mCherry by FRET detection in BMDMs. (A) Schematic of the donor control (HSA–AF488 labeled endosome) in the absence of FcRn–mCherry and the FRET experiment (HSA–AF488 and rHSA^{H464Q}–AF488-labeled endosome, donor, in the presence of FcRn–mCherry, acceptor). (B, C) Intensity images of parental BMDMs incubated for 20 min with either HSA–AF488 only (donor control) or FcRn–mCherry expressing BMDM incubated for 20 min with either HSA–AF488 or rHSA^{H464Q}–AF488 (FRET experiment) in the donor, B, and acceptor, C, channel. (D) Combined phasor distribution of HSA–AF488 and rHSA^{H464Q}–AF488 (donor) lifetimes in the absence or presence of FcRn–mCherry (acceptor) with a theoretical FRET trajectory for the donor control (3.2 ns; centered within the teal cursor) and for moderate FRET (2.5 ns) (centered within the red cursor). The distribution of pixel lifetimes is shown as a heat map. The FRET trajectory identifies the efficiency of interaction between HSA–AF488 and FcRn–mCherry after 20 min incubation to be 21%. The 20-min time point was used to quantify and spatially map the degree of HSA versus HSA^{H464Q} interaction with FcRn in BMDM (Figure 7). (E, F) Quantitation of the number of pixels undergoing FRET, E in FLIM images (f) of the donor control ($N = 8$ measurements across four cells) versus HSA–AF488 ($N = 20$ measurements across six cells) and rHSA^{H464Q}–AF488 ($N = 21$ measurements across five cells) in the presence of FcRn–mCherry (FRET experiment); F, panels are matched to A and reveals only wt HSA to undergo significant interaction with FcRn–mCherry. The pseudo-color coding (teal or red) of the images in F is linked to the pixel lifetimes on the phasor plot. Scale bar, 5 μm. The box and whisker plots in E show minimum, maximum, sample median, and first and third quartiles. The data were analyzed by an unpaired two-tailed Student *t* test, $*p < 0.05$.

interactions of receptors with ligands in vivo. The biophysical approaches used here provide a convenient in vivo assay to quantify receptor interactions. FFS has increasingly been utilized to study the dynamic behavior of macromolecules in cells, and our study expands the potential of this approach to determine the dynamics of ligand interactions within the lumen of the endosomal system. The use of these biophysical techniques to probe interactions within primary cells has broad application in a variety of physiological systems, such as receptor signaling mediated by ligand interactions with intracellular toll-like receptors in endosomes, ligand activation of G-protein coupled receptors within the endosomal system, intracellular interactions of cargo with cargo receptors, and loading of antigens onto MHC molecules with specialized endosomal loading compartments.

MATERIALS AND METHODS

Request a protocol through *Bio-protocol*.

Antibodies and reagents

Affinity-purified rabbit polyclonal antibodies to FcRn (#HPA012122; 1:200) were purchased from Atlas Antibodies (Sweden). Mouse antibodies to α-tubulin (Clone 236-10501) and DAPI (4′,6-diamidino-2-phenylindole, dihydrochloride) were purchased from Life Technologies (Grand Island, NY, USA). Mouse monoclonal antibodies to

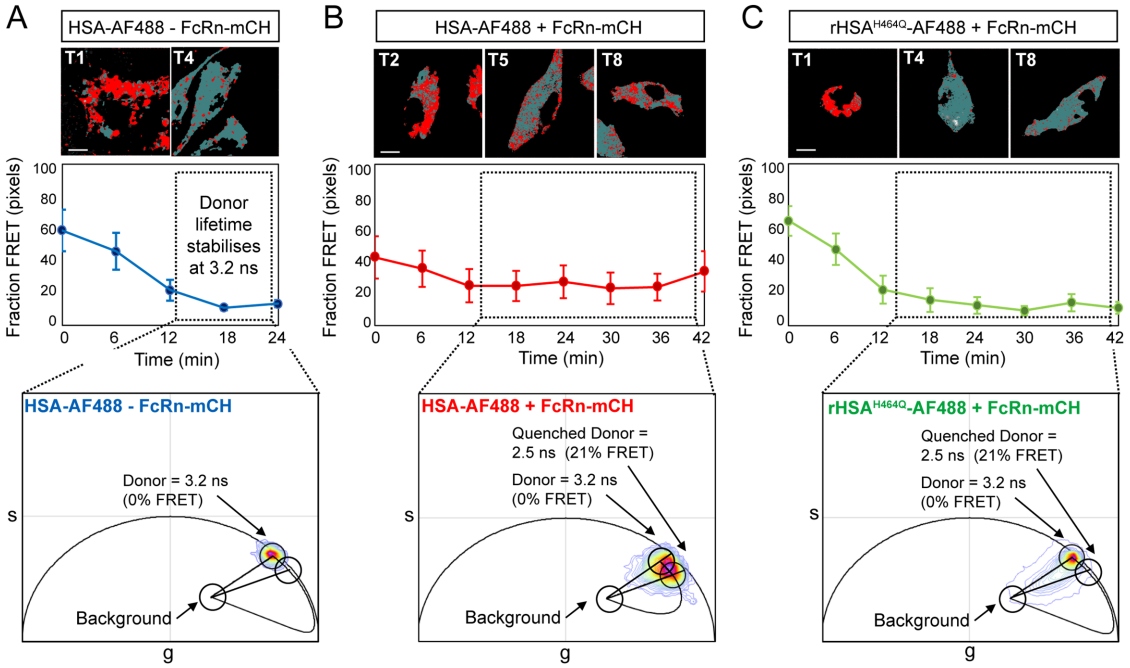

FIGURE 7: Time course of FLIM of HSA–Alexa488 in live BMDM in the presence and absence of FcRn-mCherry. FcRn KO BMDM were either untransduced or transduced with recombinant FcRn–mCherry lentivirus as described in *Materials and Methods* and incubated with 100 µg/ml HSA–AF488. (A) FLIM images of HSA–AF488 in the absence of FcRn–mCherry as a function of time ($N = 4$) reveals the fluorescence lifetime of AF488 to stabilize at 3.2 ns after 20 min incubation. This is the fluorescence lifetime used to extrapolate the FRET trajectory along the universal circle. FRET in images shown by the red pseudo-color, unquenched donor by the teal pseudo-color. On images, T1 = 1 min, T4 = 18 min. (B) FLIM images of HSA–AF488 in the presence of FcRn–mCherry as a function of time ($N = 6$ cells) reveal the efficiency of FRET interaction between HSA and FcRn to be 21% (i.e., quenched lifetime 2.5 ns) after 20 min incubation. On images, T2 = 6 min, T5 = 24 min, T8 = 42 min. (C) FLIM images of rHSA^{H464Q}–AF488 in the presence of FcRn–mCherry as a function of time ($N = 5$ cells) demonstrate a similar initial change in fluorescence lifetime to the donor control that stabilizes after 20 min incubation. On images, T1 = 0 min, T4 = 18min, T8 = 42 min. A negligible FRET interaction is detected between rHSA^{H464Q} and FcRn. Error bars indicate SEM.

Rab11 (BD610656) and GM130 (BD610823) were purchased from BD Biosciences. Mouse monoclonal antibodies to CD63 (MX-49.129.5, IgG) were purchased from Santa Cruz (USA) and mouse monoclonal antibodies to KDEL (ADI-VAA-PT048) and KDEL receptor (ADI-SPA-827) were purchased from Enzo Life Sciences (USA). Rabbit polyclonal antibodies to mCherry were from Abcam (ab183628), mCSF-1 (GF053) was purchased from Merck Millipore (Bayswater, VIC, Australia). Laboratory generated rabbit anti-SNX5 antibody has been described previously (Lim *et al.*, 2012). Secondary antibodies used for immunofluorescence were purchased from Life Technologies. Horseradish peroxidase (HRP)-conjugated sheep Anti-Rabbit Ig, Anti-mouse Ig, and donkey Anti-goat Ig were purchased from ThermoFischer (Australia).

Plasma-derived HSA was labeled with Alexa Fluor 488 (AF488) NHS ester (succinimidyl ester; Life Technologies, A-20000) or Alexa Fluor 568 (AF568) NHS ester (succinimidyl ester; Life Technologies, A-37572), respectively, according to the manufacturer's protocol. Recombinant FcRn nonbinding albumin variant HSA^{H464Q} was generated and labeled with Alexa Fluor 488 (AF488) NHS ester (succinimidyl ester; Life Technologies, A-20000; rHSA^{H464Q}-488).

Cell culture

HeLa cells, verified by genomic sequencing, were maintained in a 10% CO_2 37°C humidified incubator as adherent semiconfluent monolayers in complete DMEM (c-DMEM) supplemented with 10% (vol/vol) fetal bovine serum (FBS), 2 mM L-glutamine, and 100 units/µl of penicillin and 0.1% (wt/vol) of streptomycin (c-DMEM). Cells were routinely tested for mycoplasma contamination using a MycoAlert mycoplasma detection kit (Lonza, Switzerland).

Mice

FcRn$^{-/-}$ mice, which harbor a knockout allele of the mouse FcRn α-chain (*Fcgrt*^{tm1Dcr}), and FcRn –/– hFcRn (line 276) Tg mice (hFcRn$^{Tg/Tg}$), which have the null mutation for the mouse FcRn gene and a transgene expressing the human FcRn α-chain under the control of the β-actin promoter (Chaudhury *et al.*, 2003), were purchased from Jackson Laboratory (Bar Harbour, ME) and mouse colonies were established and maintained under specific pathogen-free conditions in the animal facility of Bio21 Institute, University of Melbourne. All experiments carried out on animals were approved by the institutional Animal Care and Use Committee.

Isolation of primary mouse bone marrow–derived macrophages

mFcRn$^{-/-}$ (FcRn KO) and hFcRn$^{Tg/Tg}$ mice 8 to 10 wk old were killed by CO_2 asphyxiation and BMDMs were generated as previously described (Lim *et al.*, 2012; Toh *et al.* 2019). Cells were seeded in 35-mm µ-dishes (Ibidi, Germany) at 0.6×10^5 cells/dish.

Generation of FcRn–mCherry constructs

To generate FcRn tagged at the C-terminus with mCherry, the coding sequence of the heavy chain of the human FcRn alpha chain was

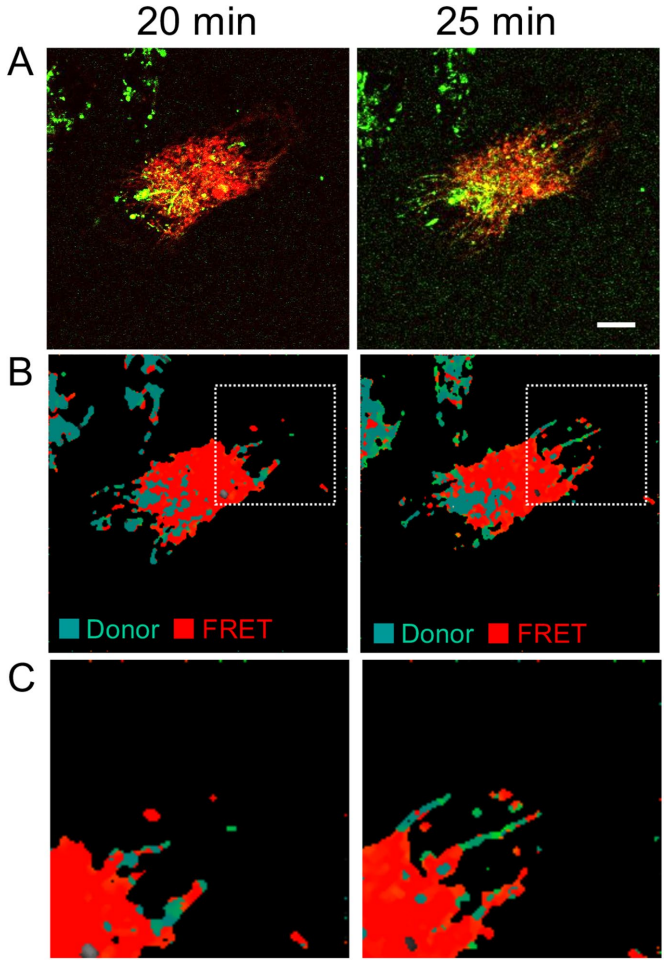

FIGURE 8: FLIM of HSA–AF488 in FcRn positive tubules. FcRn–mCherry transduced FcRn-KO BMDM were activated with CSF-1 to induce macropinocytosis, pulsed with HSA–AF488 for 5 min, and chased for up to 25 min. Shown are images at 20 and 25 min. (A) fluorescent intensity images and (B, C) FLIM map with detection of FRET in tubular structures C are enlarged images of boxed regions in B. Scale bar, 10 µm.

cloned into the pEF1α-mCherry-N1 (Clontech) using the *Age*I site in the MCS. A flexible linker (Ala–Arg–Asp–Pro–Pro–Val–Ala–Thr) was included to enhance the correct folding of FcRn and mCherry of the fusion protein. An ER signal peptide was included at the 5′ end. FcRn–mCherry sequences were amplified and cloned into pIRES vector with human β2-microglobulin, the latter inserted upstream of the IRES, resulting in the polycistronic plasmid pIRES–B2M–FcRn–mCherry expressing both β2-microglobulin and FcRn–mCherry under the control of the same promoter. B2M–FcRn–mCherry (C-terminal tagged) construct from pIRES–B2M–FcRn–mCherry was also cloned into the *Eco*RI–*Bam*HI sites of the lentiviral vector pFUGW used for transductions.

FcRn tagged at the N-terminus with mCherry (mCherry–FcRn) was also generated in pIRES vector with the linker Ala–Arg–Asp–Pro–Pro–Val–Ala–Thr between mCherry and FcRn, designated pIRES–B2M–mCherry–FcRn.

Generation of lentivirus and transduction of bone marrow–derived macrophages

Recombinant lentivirus particles were generated and used for transduction of primary BMDMs as previously described (Lim *et al.*, 2015; Toh *et al.*, 2019). Briefly, lentivirus was generated via calcium phosphate transfection of the HEK293T packaging cells with lentiviral plasmids at a weight ratio of 1 pCMV-VSV-G:2 psPAX2:2 FcRn transfer vector. Cells were transfected overnight, the medium was then replaced, and cells were incubated for a further 48 h to allow the production of viral particles. Virus-containing medium was harvested and centrifuged to pellet cell debris, and the viral supernatant was filtered using a Steriflip-HV sterile centrifuge tube top filter unit (Merck). PEG-it virus precipitation solution (Integrated Sciences, Australia) was added to the filtered viral medium at 1× final concentration and incubated overnight at 4°C. Viral particles were pelleted by centrifugation and resuspended in serum-free RPMI supplemented with 10 mM HEPES (Life Technologies, Thermo Fisher Scientific) at 1:100 of its original harvested volume. Concentrated virus was allocated into cryovials, snap frozen on dry ice, and stored at –80°C.

BMDMs were transduced with 15-µl/well (µ-dishes, Ibidi) of lentivirus diluted with fresh complete RPMI medium (Roswell Park Memorial Institute media supplemented with 10% [vol/vol] FBS, 2 mM GlutaMax, and 100 units/µl penicillin and 0.1% streptomycin) to a final volume of 1.2 ml/well. Transduced cells were incubated for 24 h in a 37°C incubator with 5% CO_2, followed by replacement of lentiviral medium with fresh complete RPMI medium and incubated for a further 24 h. BMDMs were starved for CSF-1 in complete RPMI medium overnight the day before the experiment.

Human serum albumin uptake assays

To determine the pH specificity of HSA binding to FcRn/mCherry fusion proteins, semiconfluent HeLa cells were transfected with the FcRn–mCherry constructs and then 48 h later binding and uptake assays were performed as described by Chia *et al.* (2018), at the pH indicated with 100 µg/ml HSA-AF488.

BMDMs were initially cultured overnight in the absence of CSF-1 to render the macrophages quiescent. On the next day, monolayers were washed with PBS buffer three times and pulsed with HSA–AF488 and/or $rHSA^{H464Q}$-AF488 (100 µg/ml) diluted in serum-free RPMI supplemented with 100 ng/ml mCSF-1 for 5 min at 37°C. Cell monolayers were then washed with SFM–RPMI and the fluorescent signals were chased for indicated times.

Immunofluorescence analyses

Cell monolayers were fixed in 4% paraformaldehyde (PFA; Wako Pure Chemical Industries, Japan) for 15 min at room temperature (RT) and quenched in 50 mM NH_4Cl/PBS for 10 min at RT. For intracellular staining, fixed cells were also permeabilized with 0.1% vol/vol Triton X-100/PBS for 4 min at RT and blocked in blocking solution (5% vol/vol FBS and 0.02% vol/vol sodium azide, in PBS) for 30 min to reduce nonspecific binding, and staining was performed as described (Toh *et al.*, 2019). For staining with mouse anti-Rab11 antibodies, semiconfluent monolayers were fixed with ice-cold 10% (vol/vol) trichloroacetic acid (TCA) in PBS for 10 min on ice and quenched with 30 mM (wt/vol) glycine in PBS for 10 min at room temperature, followed by incubation with the Rab11 antibodies, diluted in Can Get Signal A (Toyobo, Japan), for 2 h. Images were acquired sequentially for multicolor imaging on a laser confocal scanning microscope (Leica TCS SP8 confocal imaging system) using a 63 × 1.4 NA HCX PL APO CS oil immersion objective and a Leica HyD photodetector. Alexa Fluor 488 was excited using the 488-nm line source of an argon laser. Alexa Fluor 568 and mCherry were excited with the 543-nm laser line of a helium–neon (HeNe) laser. DAPI was excited with a 405-nm UV laser.

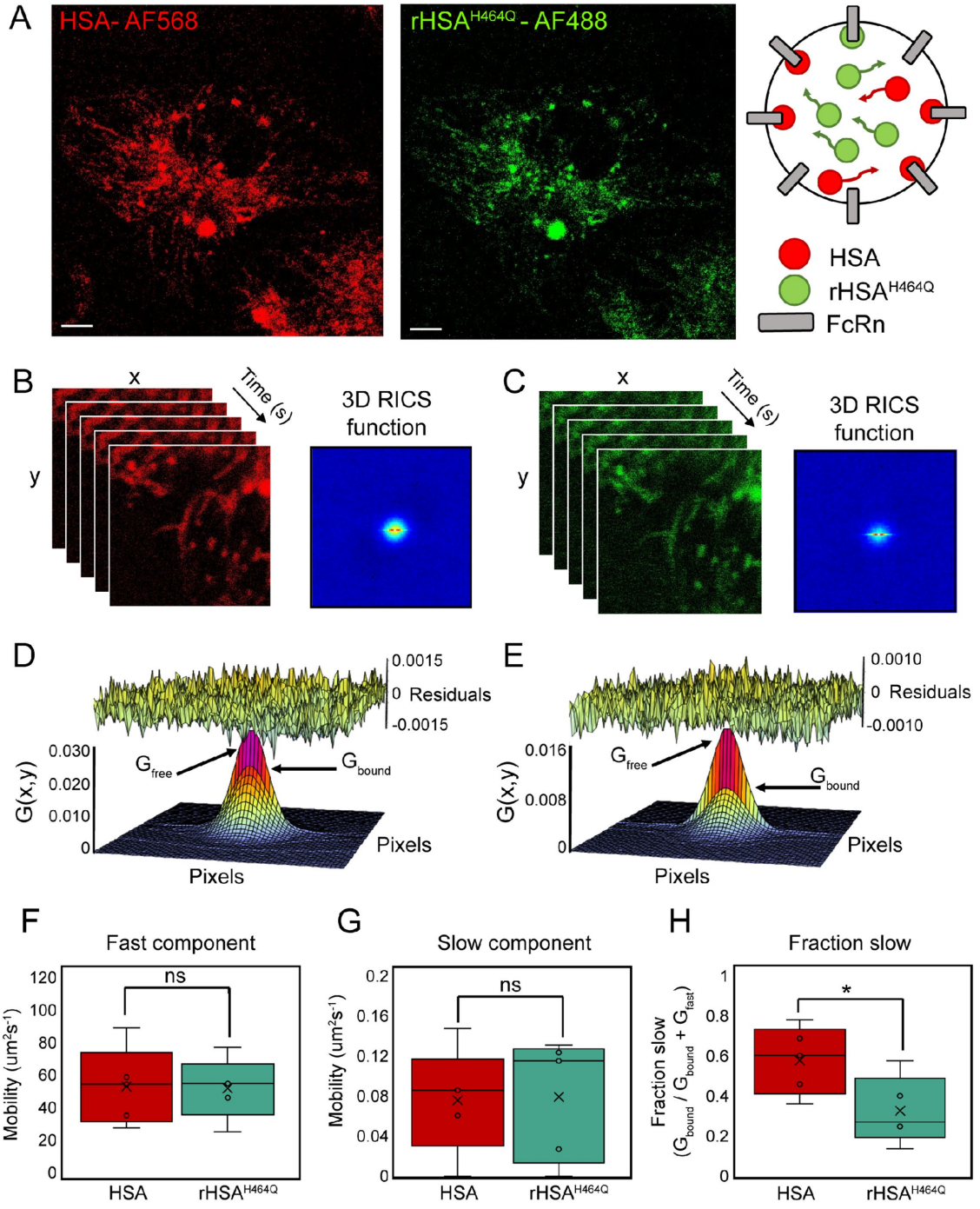

FIGURE 9: RICS of HSA–AF568 versus rHSA^{H464Q}–AF488 uptake dynamics in moving endocytic vesicles. (A) Confocal images of CSF-stimulated BMDMs incubated for 15–30 min with 10 μg/ml both HSA–AF568 and rHSA^{H464Q}–AF488 (Scale bar, 5 μm) alongside a schematic of HSA (red) versus BM (green molecules) inside a moving vesicle engaging with the FcRn receptor (grey rectangles). (B,C) Two-channel RICS data acquisition involves recording a time series of frames in the HSA–AF568 channel (red), B, versus rHSA^{H464Q}–AF488 channel (green), C, and spatiotemporal correlation of the pixels within each frame, which upon averaging gives rise to two three-dimensional (3D) RICS profiles. (D, E) The 3D RICS profile, derived from measurement of the HSA–AF568 versus rHSA^{H464Q}–AF488 mobility, fit a two-component diffusion model. Residuals of the fit are shown above the profile. G_{free} is the amplitude of the component describing free diffusion and G_{bound} is the amplitude of the component describing the bound component. (F, G) Apparent diffusion coefficient (D) of the fast (freely diffusing), F, versus slow (FcRn bound), G, component of HSA–AF568 and rHSA^{H464Q}–AF488 mobility. (H) Fraction of HSA–AF568 and rHSA^{H464Q}–AF488 exhibiting slow mobility (FcRn bound). In panels (F–H), $N = 5$ cells and the box and whisker plots show the minimum, maximum, sample median, and first and third quartiles. The means are shown by a cross. The data were analyzed by unpaired two-tailed Student's t test. *$p < 0.05$.

Fluorescence lifetime imaging microscopy (FLIM) data acquisition for detection of Förster resonance energy transfer (FRET)

All FLIM-FRET microscopy measurements were performed on an Olympus FV3000 laser scanning microscope coupled to a 488-nm pulsed laser operated at 20 MHz and an ISS A320 FastFLIM box for lifetime detection. A 60× water immersion objective (1.2 NA) was used for all experiments and live cells were imaged at 37°C degrees under 5% CO_2. To first verify the presence of HSA–AF488 (donor) and FcRn–mCherry (acceptor) in a selected BMDM cell, a sequential intensity image of this FRET pair was acquired via use of internal solid-state laser diodes operating at 488 and 561 nm, a 405/488/561 dichroic mirror, and two internal GaAsP photomultiplier detectors set to collect the following bandwidths: 500–550 nm and 600–650 nm. Then a FLIM image (256 × 256 pixel frame size, 20 µs/pixel, 90 nm/pixel, 20-frame integration) was acquired of the donor only (HSA–AF488) via use of the external pulsed 488-nm pulsed laser (20 MHz), and the resulting fluorescence signal was directed through a 405/488/561 dichroic mirror as well as a 550-nm long pass filter to an external photomultiplier detector (H7422P-40, Hamamatsu) fitted with a 520/50-nm bandwidth filter. The FLIM image of HSA–AF488, our readout of FRET with FcRn–mCherry, was processed by the ISS Vista Vision software, which precalibrates the instrument and phasor space against a known reference lifetime (here we used fluorescein at pH 9, which has a known single exponential lifetime of 4.04 ns).

The phasor approach to FLIM-FRET data analysis

All FLIM-FRET data were analyzed in the SimFCS software developed at the Laboratory for Fluorescence Dynamics, as described in previously published papers (Digman *et al.*, 2008; Hinde *et al.*, 2012). In particular, the donor fluorescence lifetime recorded in each pixel of a FLIM image is described by G and S coordinates (phasor) presented in the phasor plot. In pixels where a donor molecule undergoes FRET with an acceptor molecule, the phasor coordinate will be right-shifted along a curved trajectory that is described by the classical definition of FRET efficiency. To determine the efficiency of the FRET state, the phasor coordinates of HSA–AF488 in the absence of acceptor (unquenched donor) and background (cellular autofluorescence) were first determined independently and a FRET trajectory was extrapolated. Then from superimposition of the phasor distribution of HSA–AF488 in the presence of the C-terminal versus N-terminal FcRn fusion with mCherry (quenched donor) over the FRET trajectory, the efficiency of each ligand–receptor interaction was determined. This analysis then also enabled cursors to be placed at specific phasor coordinates along the FRET trajectory that quantify the fraction of FRET (ligand–receptor interaction) within a FLIM image and highlight this signal's spatial distribution.

Confocal microscopy data acquisition for raster image correlation spectroscopy (RICS)

All RICS microscopy measurements were performed on an Olympus FV3000 laser scanning microscope coupled to an ISS A320 Fast FLIM box for fluorescence fluctuation data acquisition. A 60× water immersion objective (1.2 NA) was used for all experiments, and live cells were imaged at 37°C degrees under 5% CO_2. HSA–AF568 and $rHSA^{H464Q}$–AF488 were excited by solid-state laser diodes operating at 488 and 561 nm, respectively. The fluorescence signal was directed through a 405/488/561 dichroic mirror to remove laser light and the Alexa488 versus Alexa568 emission was detected by two internal GaAsP photomultiplier detectors set to collect between the following bandwidths: 500–540 nm and 600–700 nm. A two-channel frame scan acquisition (100 frames) was then set-up to collect Alexa488 and Alexa568 signal at zoom 20 (10.76 μm^2 region of interest) within a selected macrophage cell that avoided free dye in the extracellular matrix. For a 256-pixel frame size this region of interest resulted in a pixel size of 41 nm and for a pixel dwell time set to 12.5 µs this scan rate resulted in a line time of 4.313 ms and a frame time of 1.108 s.

Data analysis for RICS

RICS data were processed and analyzed in the SimFCS software developed at the Laboratory for Fluorescence Dynamics, as described in previously published papers (Digman *et al.*, 2005; Digman and Gratton, 2009; Rossow *et al.*, 2010). In particular, for each two-color experiment, the RICS function was calculated in channel 1 ($rHSA^{H464Q}$–AF488) and channel 2 (HSA–AF568) for an entire image stack ($n = 100$ frames) with a moving average applied ($n = 10$ frames) to remove slow macromolecular movements. The resulting RICS profiles in channel 1 and 2 were then independently fitted to a two-component diffusion model, and the amplitudes (G_1 and G_2) versus diffusion coefficients (D_1 and D_2) of the fast versus slow components were recorded. The fast component (described by G_1 and D_1) was interpreted to represent the fraction of HSA diffusing freely, while the slow component (described by G_2 and D_2) was interpreted to represent the fraction of HSA FcRn bound.

Immunoblotting

Cellular lysates were extracted using radioimmunoprecipitation lysis buffer (50 mM Tris-HCl, pH 7.3, 150 mM NaCl, 0.1 mM EDTA, 1% wt/vol sodium deoxycholate, 1% vol/vol Triton X-100, 0.2% wt/vol NaF, and 100 µM Na_3VO_4) supplemented with 1X cOmplete mini protease inhibitor mixture (Roche Applied Science, Sigma, and Merck), and immunoblotted as described (Toh *et al.*, 2019).

Statistical analyses

Statistical analysis was performed using the unpaired *t* test in GraphPad Prism software.

ACKNOWLEDGMENTS

Confocal microscopy was performed at the Biological Optical Microscopy Platform (BOMP) at the University of Melbourne. This work was supported by funding by an Australian Research Council. Linkage Grant (LP16010373) between the University of Melbourne and CSL Limited. AP is supported by a University of Melbourne International Postgraduate Award. We gratefully acknowledge Wei Hong Toh and members of the Gleeson laboratory for valuable discussions, and Shirley Taylor (CSL) for the generation of HSA fluorescent conjugates.

REFERENCES

Andersen JT, Dalhus B, Cameron J, Daba MB, Plumridge A, Evans L, Brennan SO, Gunnarsen KS, Bjoras M, Sleep D, Sandlie I (2012). Structure-based mutagenesis reveals the albumin-binding site of the neonatal Fc receptor. Nat Commun 3, 610.

Begarani F, D'Autilia F, Signore G, Del Grosso A, Cecchini M, Gratton E, Beltram F, Cardarelli F (2019). Capturing metabolism-dependent solvent dynamics in the lumen of a trafficking lysosome. ACS Nano 13, 1670–1682.

Chaudhury C, Mehnaz S, Robinson JM, Hayton WL, Pearl DK, Roopenian DC, Anderson CL (2003). The major histocompatibility complex-related Fc receptor for IgG (FcRn) binds albumin and prolongs its lifespan. J Exp Med 197, 315–322.

Chia J, Louber J, Glauser I, Taylor S, Bass GT, Dower SK, Gleeson PA, Verhagen AM (2018). Half-life extended recombinant coagulation factor IX albumin fusion protein is recycled via the FcRn-mediated pathway. J Biol Chem 293, 6363–6373

Cullen PJ, Steinberg F (2018). To degrade or not to degrade: mechanisms and significance of endocytic recycling. Nat Rev Mol Cell Biol 19, 679–696.
Digman MA, Brown CM, Sengupta P, Wiseman PW, Horwitz AR, Gratton E (2005). Measuring fast dynamics in solutions and cells with a laser scanning microscope. Biophys J 89, 1317–1327.
Digman MA, Caiolfa VR, Zamai M, Gratton E (2008). The phasor approach to fluorescence lifetime imaging analysis. Biophys J 94, L14–L16.
Digman MA, Gratton E (2009). Analysis of diffusion and binding in cells using the RICS approach. Microsc Res Tech 72, 323–332.
Digman MA, Gratton E (2011). Lessons in fluctuation correlation spectroscopy. Annu Rev Phys Chem 62, 645–668.
Gangloff M (2012). Different dimerisation mode for TLR4 upon endosomal acidification? Trends Biochem Sci 37, 92–98.
Hanyaloglu AC (2018). Advances in membrane trafficking and endosomal signaling of G protein-coupled receptors. Int Rev Cell Mol Biol 339, 93–131.
Hinde E, Digman MA, Welch C, Hahn KM, Gratton E (2012). Biosensor Forster resonance energy transfer detection by the phasor approach to fluorescence lifetime imaging microscopy. Microsc Res Tech 75, 271–281.
Lim JP, Gleeson PA (2011). Macropinocytosis: an endocytic pathway for internalising large gulps. Immunol Cell Biol 89, 836–843.
Lim JP, Gosavi P, Mintern JD, Ross EM, Gleeson PA (2015). Sorting nexin 5 selectively regulates dorsal-ruffle-mediated macropinocytosis in primary macrophages. J Cell Sci 128, 4407–4419.
Lim JP, Teasdale RD, Gleeson PA (2012). SNX5 is essential for efficient macropinocytosis and antigen processing in primary macrophages. Biol Open 1, 904–914.
Martin WL, West AP Jr, Gan L, Bjorkman PJ (2001). Crystal structure at 2.8 A of an FcRn/heterodimeric Fc complex: mechanism of pH-dependent binding. Mol Cell 7, 867–877.
Priest DG, Solano A, Lou J, Hinde E (2019). Fluorescence fluctuation spectroscopy: an invaluable microscopy tool for uncovering the biophysical rules for navigating the nuclear landscape. Biochem Soc Trans 47, 1117–1129.
Racine E, Bell E (2008). Clinical and public translation of neuroimaging research in disorders of consciousness challenges current diagnostic and public understanding paradigms. Am J Bioeth 8, 13–15.
Retamal JS, Ramirez-Garcia PD, Shenoy PA, Poole DP, Veldhuis NA (2019). Internalized GPCRs as potential therapeutic targets for the management of pain. Front Mol Neurosci 12, 273.
Roopenian DC, Akilesh S (2007). FcRn: the neonatal Fc receptor comes of age. Nat Rev Immunol 7, 715–725.
Roopenian DC, Christianson GJ, Sproule TJ (2010). Human FcRn transgenic mice for pharmacokinetic evaluation of therapeutic antibodies. Methods Mol Biol 602, 93–104.
Rossow MJ, Sasaki JM, Digman MA, Gratton E (2010). Raster image correlation spectroscopy in live cells. Nature protocols 5, 1761–1774.
Tesar DB, Bjorkman PJ (2010). An intracellular traffic jam: Fc receptor-mediated transport of immunoglobulin G. Curr Opin Struct Biol 20, 226–233.
Toh WH, Louber J, Mahmoud IS, Chia J, Bass GT, Dower SK, Verhagen AM, Gleeson PA (2019). FcRn mediates fast recycling of endocytosed albumin and IgG from early macropinosomes in primary macrophages. J Cell Sci 133, jcs235416.
Ward ES, Ober RJ (2009). Chapter 4: Multitasking by exploitation of intracellular transport functions the many faces of FcRn. Adv Immunol 103, 77–115.